

Solar wind access to lunar polar craters: Feedback between surface charging and plasma expansion

M. I. Zimmerman,^{1,2} W. M. Farrell,^{1,2} T. J. Stubbs,^{1,2,3} J. S. Halekas,^{2,4} and T. L. Jackson^{1,2}

Received 12 July 2011; revised 1 September 2011; accepted 1 September 2011; published 5 October 2011.

[1] Determining the plasma environment within permanently shadowed lunar craters is critical to understanding local processes such as surface charging, electrostatic dust transport, volatile sequestration, and space weathering. In order to investigate the nature of this plasma environment, the first two-dimensional kinetic simulations of solar wind expansion into a lunar crater with a self-consistent plasma-surface interaction have been undertaken. The present results reveal how the plasma expansion into a crater couples with the electrically-charged lunar surface to produce a quasi-steady wake structure. In particular, there is a negative feedback between surface charging and ambipolar wake potential that allows an equilibrium to be achieved, with secondary electron emission strongly moderating the process. A range of secondary electron yields is explored, and two distinct limits are highlighted in which either surface charging or ambipolar expansion is responsible for determining the overall wake structure. **Citation:** Zimmerman, M. I., W. M. Farrell, T. J. Stubbs, J. S. Halekas, and T. L. Jackson (2011), Solar wind access to lunar polar craters: Feedback between surface charging and plasma expansion, *Geophys. Res. Lett.*, 38, L19202, doi:10.1029/2011GL048880.

1. Introduction

[2] The plasma environment within a lunar polar crater is thought to be governed by localized wake formation, in which the horizontally-flowing solar wind expands vertically into the crater to generate a plasma wake structure that can extend far downstream (e.g., Figure 1a) [Farrell *et al.*, 2007, 2010]. Consequently, solar wind protons can be diverted into the crater by local ambipolar wake electric fields, as well as by thermal diffusion, such that they are able to strike certain regions of the crater floor and possibly remove any accumulated volatiles by sputtering [Farrell *et al.*, 2010]. Other processes that could be critically affected by the presence of these “mini-wakes” include surface charging, electrostatic dust transport, volatile sequestration, space weathering, and dissipation of charged objects deep within the wake [Stubbs *et al.*, 2006; Farrell *et al.*, 2007; Jackson

et al., 2011]. This work investigates the plasma environment within a shadowed polar crater using the first fully two-dimensional kinetic simulations of plasma expansion in the vicinity of a charge-collecting surface.

[3] While the process of ambipolar plasma expansion is relatively well understood in the absence of charge-collecting boundaries [Crow *et al.*, 1975; Samir *et al.*, 1983; Farrell *et al.*, 1998; Mora, 2003], the effects of a charge-collecting surface on the wake are largely uncharacterized. Recent one-dimensional simulations and analytical work provided estimates of the ambipolar potential drop and ion fluxes expected within a lunar polar crater [Farrell *et al.*, 2008, 2010]. However, these models did not self-consistently account for the electric field produced by accumulated surface charge, thus neglecting the full nonlinear interaction between inflowing plasma and the surface. The present simulations improve upon previous models of crater wakes by resolving particle trajectories and electric field components in two spatial dimensions, enabling a fully self-consistent model of plasma expansion, the non-neutral “electron cloud” region [Crow *et al.*, 1975], and its interplay with charge accumulation and secondary electron emission at the surface boundary.

[4] It is found that for a range of simulated crater wake structures the local plasma environment is governed by a nonlinear feedback between accumulation of surface charge and the formation of a surface electric field. Interestingly, the strength of the feedback (and the resulting wake structure) is strongly modulated by the magnitude of secondary emission. A critical finding of these simulations is that solar wind protons can be diverted into the crater where they may play a role in the stability and inventory of volatiles at the crater floor.

2. Description of Simulations

[5] The open-source kinetic plasma code XOOPIC [Verboncoeur *et al.*, 1995] has been adapted to simulate the solar wind flowing into a shadowed, step-like polar crater. While real lunar craters have more complicated shapes, the step-like approximation is employed in order to reveal the wake physics in a simple and transparent manner. Incident particles stick to the surface and produce an electric field, thus facilitating a self-consistent plasma-surface interaction. In the present work, the effects of the interplanetary magnetic field are neglected since an average solar wind electron will undergo only ~3% of a gyro-orbit while transiting the crater depth and photoemission is also neglected since the entire simulated surface is assumed to be in shadow.

[6] Typical solar wind conditions are used in these simulations: horizontal flow speed $v_{sw} = 4 \times 10^5 \text{ m s}^{-1}$,

¹NASA Goddard Space Flight Center, Greenbelt, Maryland, USA.

²NASA Lunar Science Institute, NASA Ames Research Center, Moffett Field, California, USA.

³Center for Research and Exploration in Space Science and Technology, University of Maryland Baltimore County, Baltimore, Maryland, USA.

⁴Space Sciences Laboratory, University of California, Berkeley, California, USA.

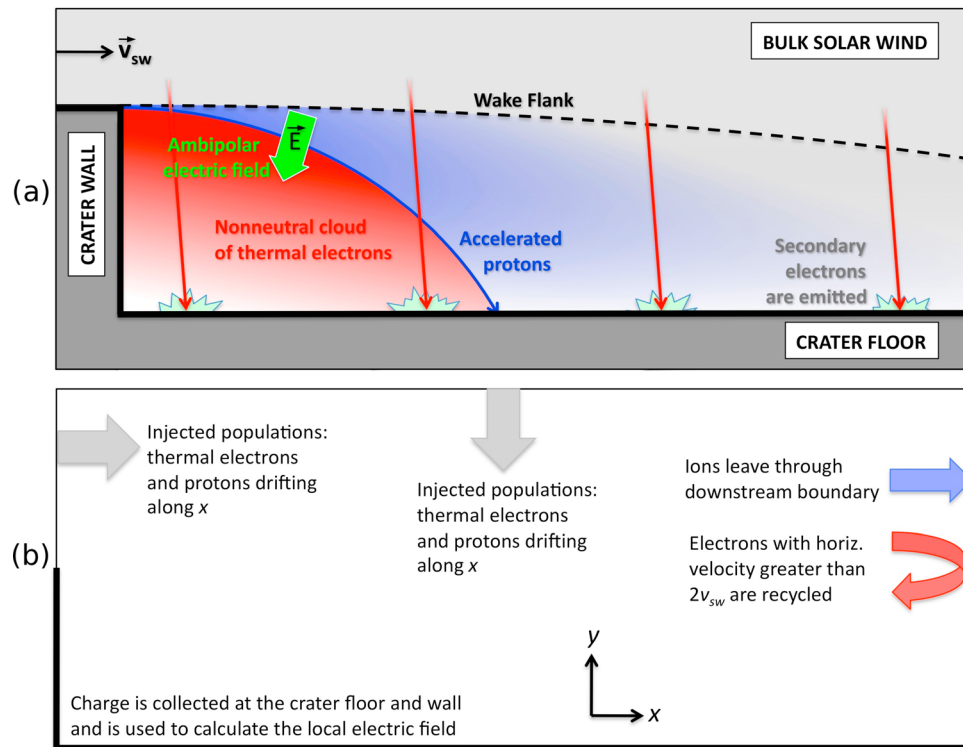


Figure 1. (a) Schematic representation of solar wind expansion into a shadowed lunar crater. (b) Overview of simulation setup.

concentration $n_0 = 5 \times 10^6 \text{ m}^{-3}$, and temperature $T_e = T_i = 11 \text{ eV}$, giving an electron thermal speed $v_{the} = 2 \times 10^6 \text{ m s}^{-1}$ and bulk plasma Debye length $\lambda_{sw} = 11 \text{ m}$. Drifting, Maxwellian electron and proton velocity distribution functions (vdf) are assumed, and a realistic electron to proton mass ratio of 1/1836 is employed. The standard simulated crater depth is $H = 500 \text{ m}$, which is representative of the common regime $H \gg \lambda_{sw}$. Electrons and protons are continuously injected at the upstream and overhead boundaries, providing a reservoir of inflowing particles to replace those which have left the simulation domain (e.g., Figure 1b). Given that $v_{the}/v_{sw} = 5$ for the conditions chosen herein, much of the electron population at the downstream boundary actually flows upstream. All electrons with horizontal velocity greater than $2v_{sw}$ that pass through the downstream boundary are recycled to model the backward moving portion of the velocity distribution, thus avoiding a charge buildup. Neumann boundary conditions are imposed upon the electric potential at the charge-collecting surface and upstream and downstream simulation boundaries, and the potential along the overhead boundary is held at 0 V.

[7] A typical simulation domain encompasses 8 km along the surface and 2 km in the vertical direction with a grid spacing of about $\lambda_{sw}/2$ (1024×256 grid points). The timestep is chosen such that the fastest electrons traverse less than one grid cell per timestep, which is about 70 times smaller than the electron plasma period of $50 \mu\text{s}$. Wake structure is insensitive to modest increases in simulation resolution, number of physical particles per computer particle, as well as simulation length and height.

[8] When noted, secondary electrons are emitted from the surface according to the empirical yield curve of Vaughan

[1989] and lunar regolith characteristics determined from Apollo samples [Willis *et al.*, 1973]. The secondary yield is isotropic and parameterized by the peak yield and the associated kinetic energy of the incident primary plasma electron, which are roughly $\delta_0 = 1.5$ and $E_0 = 300 \text{ eV}$ [Willis *et al.*, 1973], respectively. In this work the surface-wake interaction is characterized via the peak yield rather than the total yield since δ_0 is a property only of the surface and is independent of local plasma conditions.

3. Results

3.1. Plasma Expansion and Surface Interaction

[9] Figure 2a shows results from a simulation in which plasma passes unimpeded through the simulation edge that would otherwise represent the lunar surface; this scheme essentially decouples the wake from the surface and is similar to the simulation technique of Farrell *et al.* [2008]. As plasma flows horizontally into the simulation domain the faster electrons travel vertically into the void ahead of the slower-moving protons, forming a cloud of negative charge. A region of net positive charge is left behind by the vacating electrons, forming a layer of charge separation with an associated electric field along the wake flank (i.e., a double layer). Over many electron plasma periods protons enter the void through a combination of thermal diffusion and acceleration by the ambipolar field.

[10] The system eventually settles to a quasi-steady state which has four primary characteristics. First, the non-neutral electron cloud persists just downstream of the crater wall, with an electron density that falls off exponentially with distance from the wake flank. Near the crater wall, λ_{de}

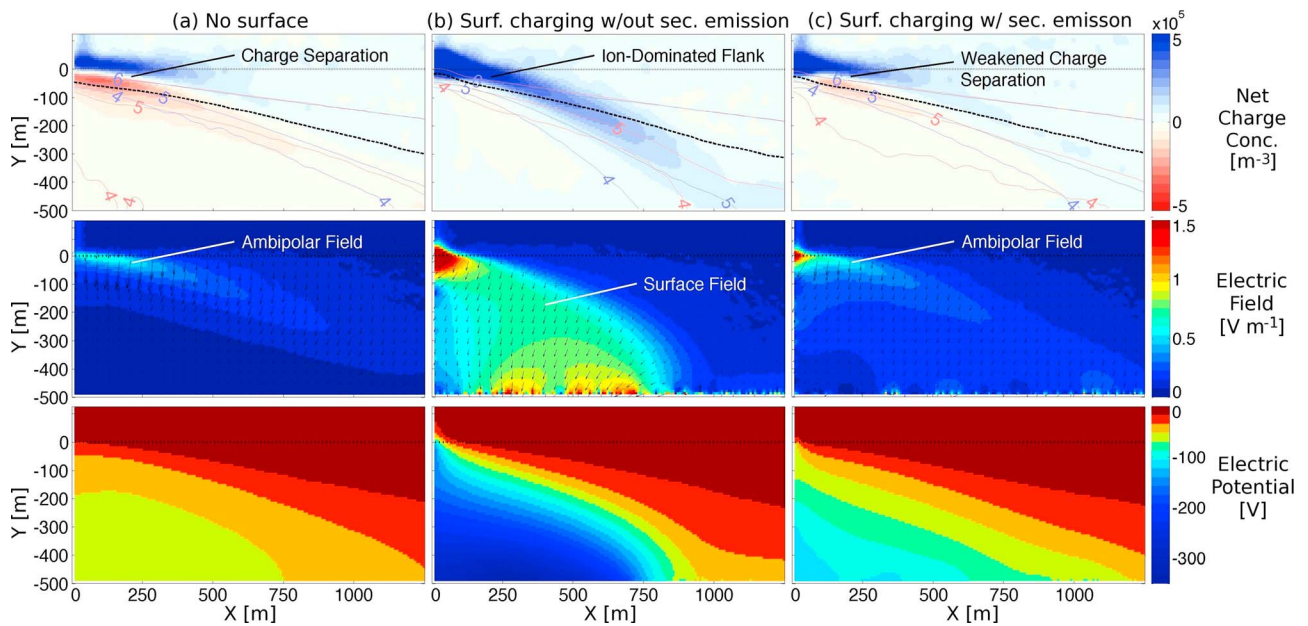


Figure 2. Fully 2D simulated plasma wake structure for a step-like lunar crater under typical solar wind conditions. (a) Open boundaries. (b) Surface charging enabled, but no secondary emission. (c) Surface charging enabled, with secondary emission ($\delta_0 = 1.5$). In the top row, red and blue correspond respectively to negative and positive charge density perturbations, with contours representing \log_{10} net concentration and black dashed contours denoting the spatial boundary along which the local Debye length is equal to $H/8$.

increases with vertical distance into the crater, rapidly becoming larger than the crater depth. Second, the ambipolar electric field structure is persistent and decreases in strength with distance downstream as the proton and electron densities begin to re-equilibrate. Third, the proton stream in the vicinity of the wake flank is diverted from its prior direction of flow. Although the proton density is significantly reduced deep within the wake, the accelerating proton front acquires a mean vertical velocity of a few multiples of the ion thermal speed ($\sim 3v_{thi}$). This is consistent with theoretical predictions that the ion front should grow more tenuous with distance into the wake, achieving a state of continuous acceleration in the non-relativistic limit [Crow *et al.*, 1975; Samir *et al.*, 1983]. Finally, the charge separation layer and electric field structure associated with the expansion process curve into the obstructed region along with the accelerated proton flow. Downstream the flank becomes less well-defined due to thermal ion diffusion.

[11] We now examine the effects of a charge-collecting dielectric surface, similar to lunar regolith, on the properties of the wake. Figure 2b shows results from a simulation in which surface charge is included in the calculation of the electric field, but secondary electrons are not emitted. At the top of the crater wall, accumulation of thermal electrons enhances the local electric field by adding a strong horizontal component. The crater floor collects electrons from the tenuous electron cloud above, floating to a large negative electric potential just downstream of the crater wall. A significant portion of the nonneutral cloud is reflected by the negative surface potential, decreasing the local electron density and increasing λ_{de} throughout most of the cloud until $\lambda_{de} > H$. Thus, the electric field associated with the accumulated surface charge is largely unshielded by the

electron cloud and so extends upward beyond the wake flank where shielding by the bulk solar wind increases rapidly with height (e.g., Figure 2b, middle). The influence of the surface electric field is, in fact, strong enough to reflect most incident electrons even at the wake flank, essentially overwhelming the local charge separation along the flank. A region of net positive charge is left in the vicinity of the wake flank, and protons in this region are accelerated into the crater under the influence of the surface electric field, although they strike the surface at some distance downstream.

[12] In the present case of Figure 2b, the electron current incident at the surface directly below the electron cloud is not balanced by a proton or secondary electron current; here, equilibrium is reached only when the surface potential becomes large enough to repel even the fastest simulated electrons ($\sim 5v_{the}$, producing a surface potential on the order of tens of T_e). In reality, perhaps another mechanism, such as negatively charged dust transport or secondary electron emission from cosmic-ray impacts, could provide current balance. Thus, the present case is representative of wake structure in the “weak secondary emission” limit (i.e., $\delta_0 \ll 1$).

3.2. Moderation of the Plasma-Surface Interaction by Secondary Emission

[13] The structure of the wake is dramatically influenced in the presence of stronger secondary emission (i.e., $\delta_0 \gtrsim 1$). Figure 2c shows results from a simulation in which the surface accumulates all incident charge but also emits secondary electrons upon impacts by solar wind electrons. In the presence of secondary emission, near the crater wall wake formation proceeds via the ambipolar expansion process and the surface potential becomes increasingly negative

as the surface collects electrons. However, the net accumulation of surface charge is moderated by the emission of secondary electrons, causing the potential to equilibrate to an intermediate level with respect to the case of Figure 2b, in which secondary emission is absent. Due to the more moderate surface potential barrier, thermal electrons are able to continuously resupply the nonneutral cloud just downstream of the crater wall, which more strongly shields the expanding solar wind from the accumulated surface charge.

[14] We have verified using a wider set of runs that there is a continuum of wake equilibria modulated by the peak secondary yield δ_0 , within which Figures 2b and 2c represent distinct structural regimes. Above the threshold $\delta_0 \sim 1.4$, secondary emission noticeably lessens the influence of surface charging on the inflowing wake plasma. In Figure 3 the total potential drop is divided into a surface component Φ_S due to accumulated charge and an ambipolar component Φ_A due to the expansion process. The spatial boundary between Φ_S and Φ_A is taken from a common vertical reference based on the local Debye length with respect to the crater depth, providing a physically consistent measure across different simulations. The relative contributions of Φ_S and Φ_A shift with the amount of secondary emission; that is, stronger secondary emission suppresses accumulation of surface charge, forming a smaller potential drop.

[15] A critical finding of these simulations is that protons are readily diverted from their horizontal trajectories toward the shadowed crater floor, comprising a significant particle flux as demonstrated in Figure 4. In cases with stronger secondary emission, protons arrive farther downstream due to the reduced magnitude and influence of the surface electric field. That solar wind protons can access shadowed lunar surfaces is significant because it is often been assumed that hydrogen-bearing volatiles sequestered in permanent shadow are topographically shielded from solar wind bombardment. A complete assessment of the nature of the

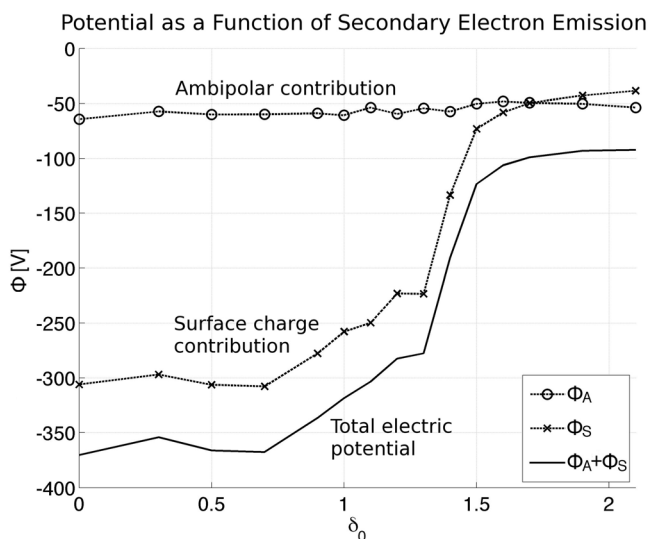


Figure 3. Components of the wake electric potential for a range of peak secondary yields. All data is taken at $x = H/2$, and the boundary between the ambipolar component Φ_A , and the surface component Φ_S , is defined to be the local height at which the Debye length is equal to $H/8$.

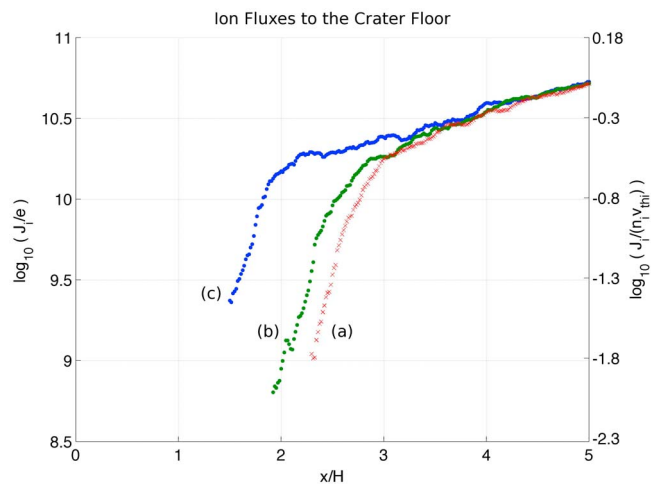


Figure 4. Quasisteady proton flux at the plane $y = -H$ for the cases of Figure 2, with (a) no charge-collecting surface, (b) a dielectric surface at $y = -H$ with peak secondary yield $\delta_0 = 1.5$, and (c) a dielectric surface at $y = -H$ with $\delta_0 = 0$. For reference, the height coordinate at the crater rim is $y = 0$.

proton-surface interaction and its implications for production and stability of lunar hydrogen is beyond the scope of the current work. However, with a physical sputtering yield on the order of one water molecule per incident proton [Johnson, 1989] a significantly icy shadowed surface could be eroded by the keV ion impacts observed in the simulations. On the other hand, for a relatively pure SiO_2 surface the physical sputtering yield for water would be quite low (~ 0.01 molecule per incident proton) [Johnson, 1989], so the expanding solar wind may represent a net source of implanted protons which could produce water or hydroxyl through various other pathways (cf. the mechanisms outlined by Crider and Vondrak [2003]). It is notable that the proton flux is negligible out to a few H downstream, suggesting that at least for a fraction of a lunation a portion of the crater floor would be shielded from proton bombardment under typical solar wind conditions. Narrow but deep polar topographic features likely provide the most persistent shielding of the lunar surface from solar wind protons.

4. Conclusions

[16] A new tool for studying the plasma wake structure within polar lunar craters was developed by adapting the publicly available kinetic plasma code XOOPIC, which can implement a self-consistent plasma-surface interaction. Wake formation was found to be predominantly ambipolar in nature, with the fastest-moving thermal electrons initially racing into the crater ahead of the protons. However, the presence of a dielectric surface (a proxy for shadowed lunar regolith) dramatically affects the wake in previously unforeseen ways. In particular, a negative feedback arises between surface charge accumulation and the inflowing solar wind to produce a quasisteady wake; this process (and the resulting electrostatic structure) is strongly moderated by the amount of secondary electron emission. A critical finding is that wake formation causes solar wind protons to be diverted toward the shadowed crater floor where they may play a role in the formation and

depletion of volatiles. The present simulations provide estimates of the properties of proton streams incident upon the surface of permanently shadowed lunar craters (e.g., Figure 4).

[17] **Acknowledgments.** This research was supported by an appointment to the NASA Postdoctoral Program at the Goddard Space Flight Center, administered by Oak Ridge Associated Universities through a contract with NASA. The support of LPROPS grant NNX08AN76G and the NASA Lunar Science Institute and DREAM virtual institute through grant NNX09AG78A are gratefully acknowledged.

[18] The Editor thanks two anonymous reviewers for their assistance in evaluating this paper.

References

- Crider, D. H., and R. R. Vondrak (2003), Space weathering effects on lunar cold trap deposits, *J. Geophys. Res.*, *108*(E7), 5079, doi:10.1029/2002JE002030.
- Crow, J. E., P. L. Auer, and J. E. Allen (1975), The expansion of a plasma into a vacuum, *J. Plasma Phys.*, *14*, 65.
- Farrell, W. M., M. L. Kaiser, J. T. Steinberg, and S. D. Bale (1998), A simple simulation of a plasma void: Applications to Wind observations of the lunar wake, *J. Geophys. Res.*, *103*, 23,653.
- Farrell, W. M., T. J. Stubbs, R. R. Vondrak, G. T. Delory, and J. S. Halekas (2007), Complex electric fields near the lunar terminator: The near-surface wake and accelerated dust, *Geophys. Res. Lett.*, *34*, L14201, doi:10.1029/2007GL029312.
- Farrell, W. M., T. J. Stubbs, J. S. Halekas, G. T. Delory, M. R. Collier, R. R. Vondrak, and R. P. Lin (2008), Loss of solar wind plasma neutrality and affect on surface potentials near the lunar terminator and shadowed polar regions, *Geophys. Res. Lett.*, *35*, L05105, doi:10.1029/2007GL032653.
- Farrell, W. M., T. J. Stubbs, J. S. Halekas, R. M. Killen, G. T. Delory, M. R. Collier, and R. R. Vondrak (2010), Anticipated electrical environment within permanently shadowed lunar craters, *J. Geophys. Res.*, *115*, E03004, doi:10.1029/2009JE003464.
- Jackson, T. L., W. M. Farrell, R. M. Killen, G. T. Delory, J. S. Halekas, and T. J. Stubbs (2011), The Discharging of roving objects in the lunar polar regions, *J. Spacecr. Rockets*, *48*, 700.
- Johnson, R. E. (1989), *Energetic Charged Particle Interactions With Atmospheres and Surfaces*, chap. 3, Spinger, New York.
- Mora, P. (2003), Plasma expansion into a vacuum, *Phys. Rev. Lett.*, *90*, 185002.
- Samir, U., K. H. Wright Jr., and N. H. Stone (1983), The expansion of a plasma into a vacuum: Basic phenomena and processes and applications to space plasma physics, *Rev. Geophys.*, *21*, 1631.
- Stubbs, T. J., R. R. Vondrak, and W. M. Farrell (2006), A dynamic fountain model for lunar dust, *Adv. Space Res.*, *37*, 59.
- Vaughan, J. R. M. (1989), A new formula for secondary emission yield, *IEEE Trans. Electron Devices*, *36*, 1963.
- Verboncoeur, J. P., A. B. Langdon, and N. T. Gladd (1995), An object-oriented electromagnetic PIC code, *Comput. Phys. Commun.*, *87*, 199.
- Willis, R. F., M. Anderegg, B. Feuerbacher, and B. Fitton (1973), Photoemission and secondary electron emission from lunar surface material, in *Photon and Particle Interactions with Space, Proceedings of the 6th ESLAB Symposium, Astrophys. Space Sci. Libr.*, vol. 37, p. 389, Reidel, Dordrecht, Netherlands.

W. M. Farrell, T. L. Jackson, and M. I. Zimmerman, NASA Goddard Space Flight Center, Code 695, Greenbelt, MD 20771, USA. (michael.i.zimmerman@nasa.gov)

J. S. Halekas, Space Sciences Laboratory, University of California, 7 Gauss Way, Berkeley, CA 94720, USA.

T. J. Stubbs, Goddard Earth Science and Technology Center, University of Maryland Baltimore County, Baltimore, MD 21228, USA.